ORIGINAL ARTICLE

Role of strain rate in the strain-induced crystallization (SIC) of natural and synthetic isoprene rubber

Yuji Kitamura[1] · Kiyoka Okada[2] · Hiroyasu Masunaga[3] · Masamichi Hikosaka[2]

Abstract

The role of strain rate ($\dot{\varepsilon}$) in the strain-induced crystallization (SIC) of vulcanized natural rubber (NR) and synthetic isoprene rubber (IR) was studied using in situ wide-angle X-ray scattering (WAXS) (synchrotron X-ray radiation). We developed homemade extension equipment and coupled it with the synchronized time-resolved X-ray detector system. The nucleation rate (I) was determined for a wide range of $\dot{\varepsilon}$ values ($0.0075 \, \text{s}^{-1}$–$330 \, \text{s}^{-1}$) based on the increase in the scattering intensity (I_X) as a function of time (t). We found that I is proportional to $\dot{\varepsilon}$ ($I \propto \dot{\varepsilon}$). Based on this result, we concluded that $\dot{\varepsilon}$ plays an important role in the kinetic mechanism of the SIC of NR and IR.

Introduction

Natural rubber (NR) and synthetic isoprene rubber (IR) are important materials in rubber science and industry because they show interesting crystallization behaviors and useful physical properties, such as crack resistance [1]. For automobile tires, NR is mainly used in the skeleton (the covering material of reinforced fibers) because it has low rolling resistance, low heat generation and enhanced durability [2]. Moreover, tires used on off-road vehicles, aircraft and other means of transportation that operate in severe conditions are primarily made of NR compounds because a high level of durability is needed [2]. Interestingly, the "strain-induced crystallization" (SIC) or "elongational crystallization" of NR has been known for a long time [3]. Katz observed the SIC of NR using wide-angle X-ray scattering (WAXS) in 1925 but did not solve the crystallization mechanism [3].

It is widely thought that in NR and IR crack propagation at the crack tip is suppressed by SIC. Lee et al. observed the crack tip utilizing WAXS. They concluded that the ability of NR to resist cracking was improved by SIC brought on by carbon black nanoparticles [4]. Le Cam et al. studied the mechanism of fatigue crack growth at the crack tip in NR by observing the fracture surface with a scanning electron microscope (SEM) [5].

Alexander et al. studied SIC using X-ray scattering in a sequential (extend and hold) manner [6]. Recently, Murakami et al. observed SIC under uniaxial extension in situ using X-ray synchrotron radiation [7]. They reported hysteresis behavior in the crystalline reflection intensity and in the orientation of amorphous during the extension and retraction process. Chenal et al. observed SIC in situ using X-rays and reported that the size of the crystallites remain constant during the SIC process [8].

Mitchell et al. measured temperature changes in NR using an embedded thermocouple to detect SIC during extension [9]; however, they did not mention the role of strain rate ($\dot{\varepsilon}$). Candau et al. studied the effect of crystallization temperature (T_c) and $\dot{\varepsilon}$ on the SIC of NR and IR utilizing WAXS [10]. Based on thermodynamic considerations, they suggested that the reason why IR crystallizes larger strain (ε), while NR does under lower ε, might be because the equilibrium melting temperature (T_m^0) of IR is lower than that of NR. While they studied the effect of the $\dot{\varepsilon}$ on the onset of crystallization, they did not investigate the

✉ Yuji Kitamura
  kitamu-y@bridgestone.com

1   Advanced Materials Development Division, Bridgestone
    Corporation, Ogawahigashi-cho 3-1-1, Kodaira City 187-8531
    Tokyo, Japan

2   Graduate School of Integrated Arts and Sciences, Hiroshima
    University, Kagamiyama 1-7-1, Higashi-hiroshima City,
    Hiroshima 739-8521, Japan

3   SPring-8, Japan Synchrotron Radiation Research Institute
    (JASRI), Kouto 1-1-1, Sayo-cho, Sayo-gun, Hyogo 679-5198,
    Japan

role of the $\dot{\varepsilon}$. Tosaka et al. observed SIC in NR and IR utilizing WAXS up to relatively large values of $\dot{\varepsilon}$ [11]. They showed that the crystallinity (χ_c) increased even after sample extension was stopped. They performed analyses at a constant ε that focused on the change in χ_c after extension, but they did not discuss the role of $\dot{\varepsilon}$ in SIC.

Okada et al. carried out kinetic studies pertaining to the SIC of synthetic linear polymers, such as isotactic polypropylene (iPP) and polyethylene terephthalate (PET) melts. They found that the nucleation rate (I) was significantly accelerated when $\dot{\varepsilon}$ becomes larger than the critical strain rate ($\dot{\varepsilon}^*$). The $\dot{\varepsilon}^*$ ranged between several to several hundred s^{-1}. They proposed that this acceleration in the I was due to the change in the structure of the melt upon elongation (isotropic melt to oriented melt) [12–14]. They also showed that SIC in iPP and PET is primarily controlled by nucleation. These studies, in which the kinetic role of $\dot{\varepsilon}$ is investigated, are unique.

To the best of our knowledge, kinetic studies looking at the SIC of NR and IR based on Classical Nucleation Theory (CNT) [15] have not yet been performed. CNT states that the "crystallization kinetic process" is divided into the nucleation and growth phases and that the nucleation process is critical to the crystallization process as a whole. CNT says that the degree to which supercooling (ΔT) is dependent upon the nucleation rate is important in kinetic crystallization mechanisms, where ΔT is defined as

$$\Delta T = T_m^0 - T_c. \tag{1}$$

CNT also provides the following relationship for nucleation-controlled crystallization processes:

$$I \propto \tau_i^{-1}, \tag{2}$$

where τ_i is the induction time [16, 17].

The vulcanized NR and IR measured in this study contain cross-linked polymer chains (linear chain synthetic polymers (iPP and PET) do not), so it is likely that the cross-linking of the polymer chains strongly influences the SIC mechanism. Therefore, it is an interesting unsolved problem to clarify how cross-linking affects the kinetic SIC mechanism.

Miyamoto et al. performed stress-strain tests of IR and suggested that in theory the SIC of IR could be controlled by nucleation [18]. However, they didn't show any experimental evidence to support that claim. Recently, we have shown that the SIC of NR is controlled primarily by nucleation based on direct measurements of the dependence of ΔT on I using WAXS [19–21].

The purposes of this work are to (1) carry out kinetic studies related to the SIC of NR and IR using in situ WAXS

Table 1 Formulation of vulcanized NR and IR samples

content	
(wt%)	
Natural rubber or isoprene rubber	88.7
Stearic acid	1.8
ZnO	4.4
Sulfur	1.3
Accelerator (CBS)	1.3
Antioxidant, etc.	2.5

CBS N-cyclohexyl benzothiazole-2-sulfenamide

for a large range of $\dot{\varepsilon}$, (2) evaluate I as a function of $\dot{\varepsilon}$ and (3) explore whether or not I significantly increases with increasing $\dot{\varepsilon}$. Based on these observations, we will clarify the roles of $\dot{\varepsilon}$ and polymer cross-linking in the SIC of NR and IR.

Materials and methods

Materials

Vulcanized NR and IR were measured. The sample formulations are shown in Table 1. Commercial natural rubber RSS#3 (Southland Rubber Co., Ltd, Hatyai, Thailand) and synthetic polyisoprene IR2200 (JSR corp., Tokyo, Japan) were used. The number-averaged molecular weight (M_n) of the IR was 6.1×10^5, and the molecular weight distribution M_w/M_n was 3.13, where M_w is weight-averaged molecular weight. The specimen was dumbbell-shaped, and the size of the flat region (without the knobs) was $3\,\text{mm} \times 3\,\text{mm} \times 1\,\text{mm}$.

Uniaxial extension

Homemade equipment that included a pair of opposite motors was used for uniaxial extension to fix the center position of the specimens [19–21]. Random dots were sprayed on the specimen surface, and then, the changes in the ε and the thickness of the specimen over time were directly measured using a video system. $\dot{\varepsilon}$ is defined as

$$\dot{\varepsilon} \equiv \frac{d\varepsilon}{dt}, \tag{3}$$

where t is the elapsed time. The starting time of the sample extension was defined as $t = 0$. In this study, $\dot{\varepsilon}$ was determined as the initial slope on the plot of ε vs. t. We observed $\dot{\varepsilon}$ values from $0.0075\,\text{s}^{-1}$ to $330\,\text{s}^{-1}$. The maximum strain (ε_{max}) was 5. SIC was observed at $T_c = 27\,°\text{C}$.

Fig. 1 Methods of WAXS analysis. **a** A typical WAXS image of extended NR. $T_c = 27\,°C$ and $\varepsilon = 5$. The integrated area is shown as a dotted line. **b** $I_X(q, \varepsilon = 5)$ was obtained by subtracting $I_X^{obs}(q, \varepsilon < 1)$ from $I_X^{obs}(q, \varepsilon = 5)$
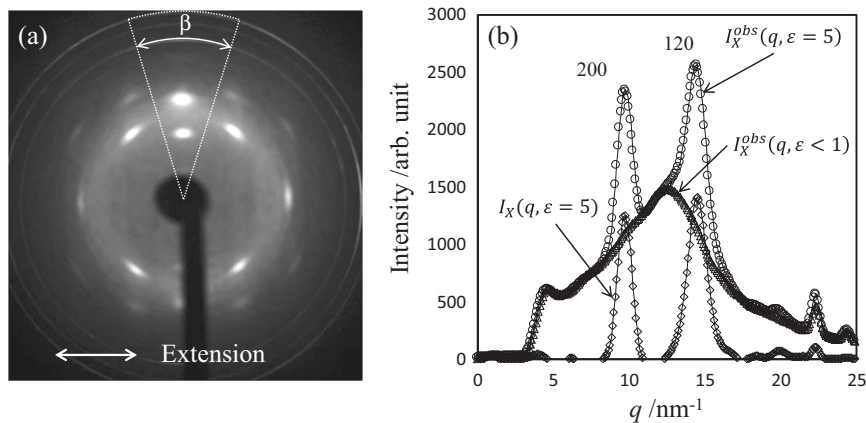
WAXS

WAXS observations were carried out using synchrotron radiation at beam line BL03XU [22, 23] of SPring-8 (Japan Synchrotron Radiation Research Institute; JASRI). The wavelength (λ) of the X-rays was 0.08 nm, and the camera length was 115 mm. A CMOS camera (Photron SA-X2) with an image intensifier (Hamamatsu Photonics V7739P/ION) was used as a detector. The detector and the X-ray shutter were synchronized with the trigger signal generated by the extension equipment. The two-dimensional (2D) WAXS patterns were recorded during sample extension. The interval of the time-resolved WAXS observations ranged from 20 s to 1 ms corresponding to $\dot{\varepsilon}$.

The X-ray scattering intensity of the observed 2D WAXS image at ε, $I_X^{obs}(q, \varepsilon)$ was obtained by integrating for $\beta = \pm 10°$, where β is the azimuthal angle and q is the scattering vector, after correcting for the dark noise of the detector, air scattering and sample thickness (Fig. 1a, b). Because reflection was not observed at $\varepsilon \leq 1$, the X-ray scattering intensity from the crystal ($I_X(q, \varepsilon)$) was obtained by

$$I_X(q, \varepsilon) \equiv I_X^{obs}(q, \varepsilon) - I_X^{obs}(q, \varepsilon \leq 1). \tag{4}$$

We focused on the peak intensity of the (200) reflection, and we notate it as $I_X(200) = I_X(q, \varepsilon)$ in this study.

Determination of I

$I_X(q, \varepsilon)$ is proportional to χ_c, that is [20, 21],

$$I_X(q, \varepsilon) \propto \chi_c, \tag{5}$$

and the size of the crystallite is constant during the SIC process [8, 19]. χ_c is proportional to the number density of nuclei (ν),

$$\chi_c \propto \nu. \tag{6}$$

From eq. (5) and (6), and the definition of CNT, I is given by

$$I = \frac{d\nu}{dt} \propto \frac{d\chi_c}{dt} \propto \frac{dI_X(q, \varepsilon)}{dt}. \tag{7}$$

Therefore, I was determined from the slope on the plot of I_X vs. t.

Results

Typical examples of plots of $I_X(200)$ vs. t ($\dot{\varepsilon} = 0.71 s^{-1}$) are shown in Fig. 2. An induction period and a steady period, where $I_X(200)$ increases linearly with increasing t, were observed after the definition of CNT [15]. τ_i was determined from the X-axis (t)-intercept of I_X in the steady period. From the slope of $I_X(200)$ in the steady period, we obtained I,

$$I \propto \frac{dI_X(200)}{dt} = 2.2 \times 10^2. \tag{8}$$

$I_X(200)$ vs. t is plotted for all $\dot{\varepsilon}$ in Figs. 3 and 4 for NR and IR, respectively. Note that SIC can be observed down to significantly small $\dot{\varepsilon}(= 7.5 \times 10^{-4} s^{-1})$. We did not observe a $\dot{\varepsilon}^*$. Similar SIC behaviors with induction and steady periods were observed for all $\dot{\varepsilon}$. I and τ_i for various $\dot{\varepsilon}$ are listed in Table 2. Plots of I vs. $\dot{\varepsilon}$ are shown in Fig. 5. We found that

$$I \propto \dot{\varepsilon} \tag{9}$$

for all observed $\dot{\varepsilon}$.

τ_i^{-1} was also plotted against $\dot{\varepsilon}$ (Fig. 6). We found that

$$\tau_i^{-1} \propto \dot{\varepsilon} \tag{10}$$

for all values of $\dot{\varepsilon}$. From equations (9) and (10), we find that

$$I \propto \tau_i^{-1}. \tag{11}$$

The dependence of I on ε at various $\dot{\varepsilon}$ for NR within the steady period is shown inFig. 7. I remained nearly constant for all values of $\dot{\varepsilon}$ and does not significantly depend on ε.

Discussion

It is well-known that the SIC of NR and IR becomes detectable when ε becomes larger than 2.5 for all values of $\dot{\varepsilon}$. This point confirmed by equation (9). As I increases with increasing $\dot{\varepsilon}$, SIC becomes detectable within a short time for large $\dot{\varepsilon}$, but over a longer time frame for small values of $\dot{\varepsilon}$.
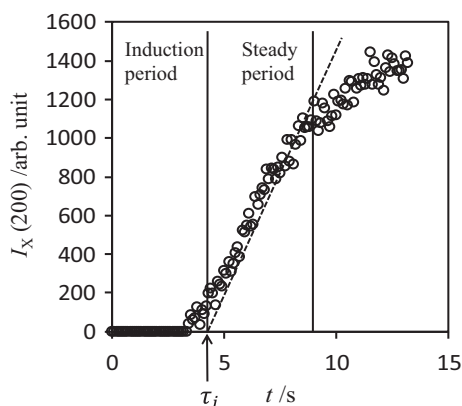
**Fig. 2** Typical plots of I_X (200) against t for NR. $T_c = 27\,°C$ and $\dot{\varepsilon} = 0.71\,s^{-1}$

Thus, it is likely that SIC can be detected at similar ε values, which does not appear to depend on $\dot{\varepsilon}$. We showed that I was almost constant for any value of $\dot{\varepsilon}$ regardless of ε (Fig. 7). This means that I is controlled by $\dot{\varepsilon}$. Therefore, the universal importance of $\dot{\varepsilon}$ in SIC has been clarified for both NR and IR and for other linear chain synthetic polymers, such as iPP and PET.

We found that for NR and IR, SIC can be observed even for significantly small $\dot{\varepsilon}(= 7.5 \times 10^{-4} s^{-1})$, and we did not observe a $\dot{\varepsilon}^*$. However, in the case of the SIC of linear chain synthetic polymers, we found that $\dot{\varepsilon}^*$ was significantly large. This difference clearly indicates that the cross-linking of polymer chains assists in the formation of the oriented melt from which nuclei are generated. Therefore, cross-linking plays an important role in the SIC of NR and IR.

Because the observed result of equation (11) was shown by CNT [16, 17], where the crystallization process is mainly controlled by nucleation, it is reconfirmed that the SIC of NR and IR is mainly controlled by nucleation processes.

Conclusions

We carried out a kinetic study of the SIC of vulcanized NR and IR over a wide range of strain rates $\dot{\varepsilon}$ (from 0.0075 s^{-1} to 330 s^{-1}) using in situ WAXS. We found important fact that the nucleation rate (I) is directly related to the strain rate
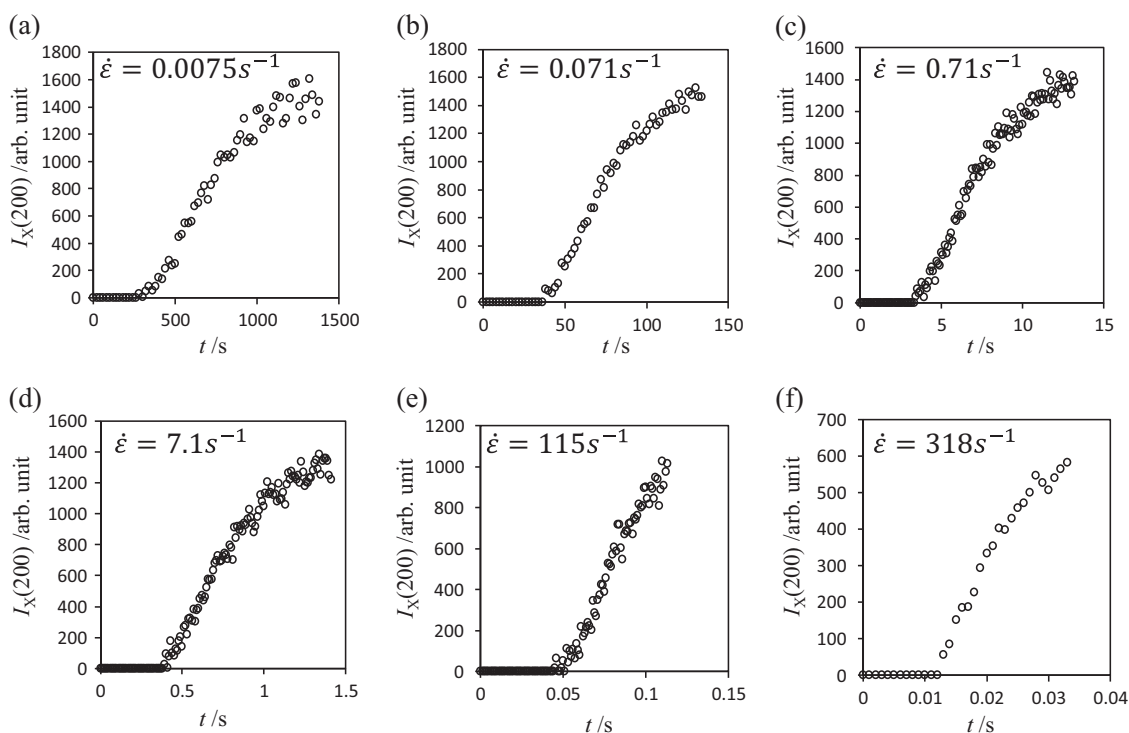
Fig. 3 Plots of I_X (200) against t for NR. **a** $\dot{\varepsilon} = 0.0075\,s^{-1}$. **b** $\dot{\varepsilon} = 0.071\,s^{-1}$. **c** $\dot{\varepsilon} = 0.71\,s^{-1}$. **d** $\dot{\varepsilon} = 7.1\,s^{-1}$. **e** $\dot{\varepsilon} = 115\,s^{-1}$. **f** $\dot{\varepsilon} = 318\,s^{-1}$
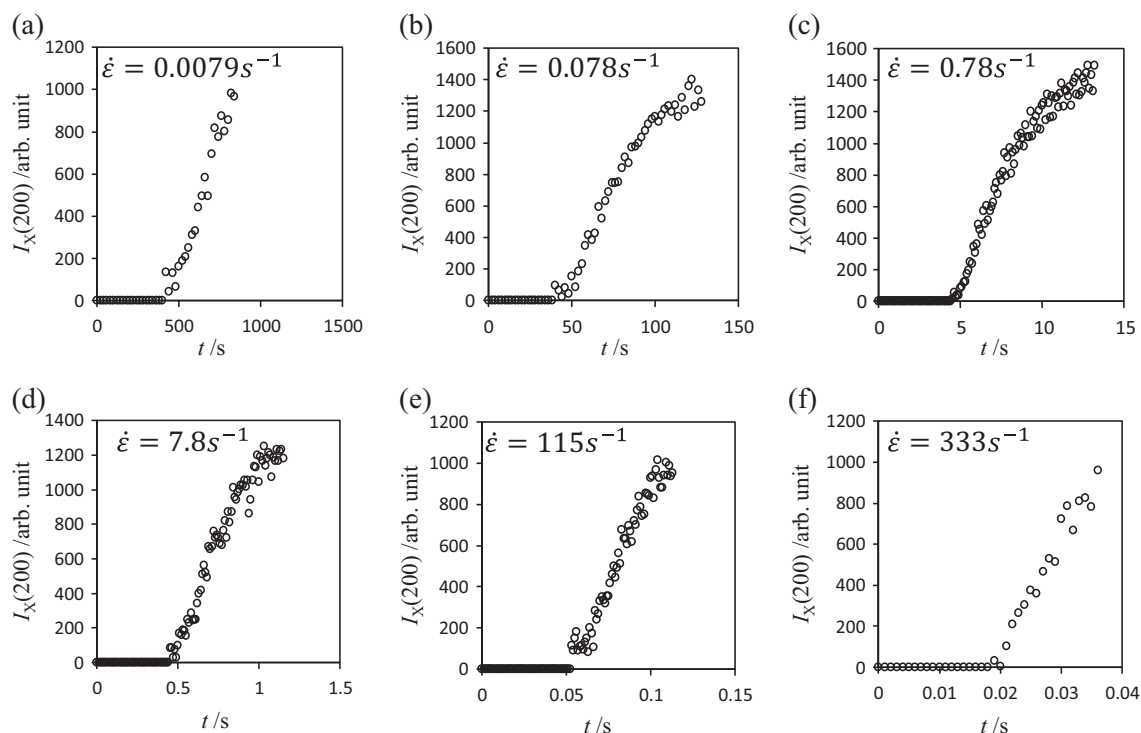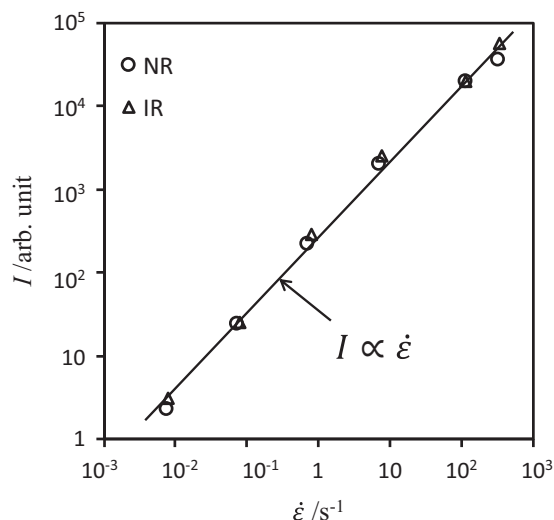
Fig. 4 Plots of I_X (200) against t for IR. **a** $\dot{\varepsilon} = 0.0079$ s^{-1}. **b** $\dot{\varepsilon} = 0.078$ s^{-1}. **c** $\dot{\varepsilon} = 0.78$ s^{-1}. **d** $\dot{\varepsilon} = 7.8$ s^{-1}. **e** $\dot{\varepsilon} = 115$ s^{-1}. **f** $\dot{\varepsilon} = 313$ s^{-1}

Table 2 I and τ_i for NR and IR

NR			IR		
$\dot{\varepsilon}$ (s^{-1})	I (arb. unit)	τ_i (s)	$\dot{\varepsilon}$ (s^{-1})	I (arb. unit)	τ_i (s)
0.0075	2.3	350	0.0079	3.1	480
0.071	24	39	0.078	25	46
0.71	220	3.6	0.78	290	4.7
7.1	2030	0.39	7.8	2600	0.47
115	20,300	0.053	115	20,000	0.055
318	36,400	0.011	333	58,000	0.019

Fig. 5 Plots of I against $\dot{\varepsilon}$. open circle indicates NR and open triangle indicates IR

($\dot{\varepsilon}$), $I \propto \dot{\varepsilon}$. Therefore, we concluded that $\dot{\varepsilon}$ plays an important role in the SIC of vulcanized NR and IR. We also did not find a critical strain rate ($\dot{\varepsilon}^*$) in contrast to studies looking at the SIC of linear chain polymers, such as iPP and PET; so, we concluded that the polymer chain cross-linking significantly assists in nucleation. We found that $I \propto \tau_i^{-1}$, where τ_i is the induction time, so we reaffirmed that the SIC of vulcanized NR and IR is mainly controlled by a nucleation process. Finally, we explained the well-known fact that the SIC of vulcanized NR and IR starts when the strain (ε) becomes larger than 2.5 (by our result that $I \propto \dot{\varepsilon}$).

Compliance with ethical standards
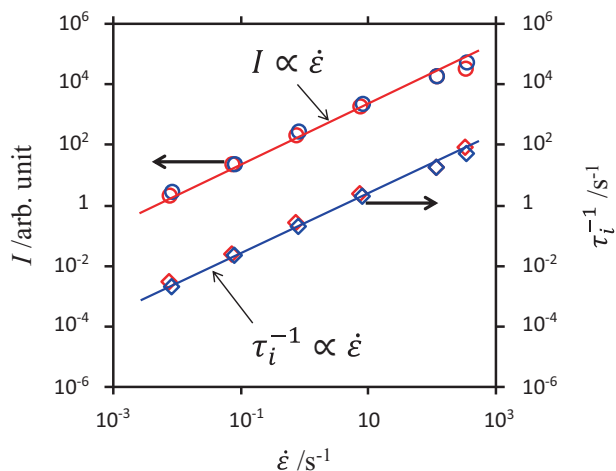
Fig. 6 Plots of I (circle) and τ_i^{-1} (diamond) against $\dot{\varepsilon}$. I and τ_i^{-1} correspond to the left and right axes, respectively. open red circle for I of NR, open blue circle for I of IR, open red diamond for τ_i^{-1} of NR and open blue diamond for τ_i^{-1} of IR
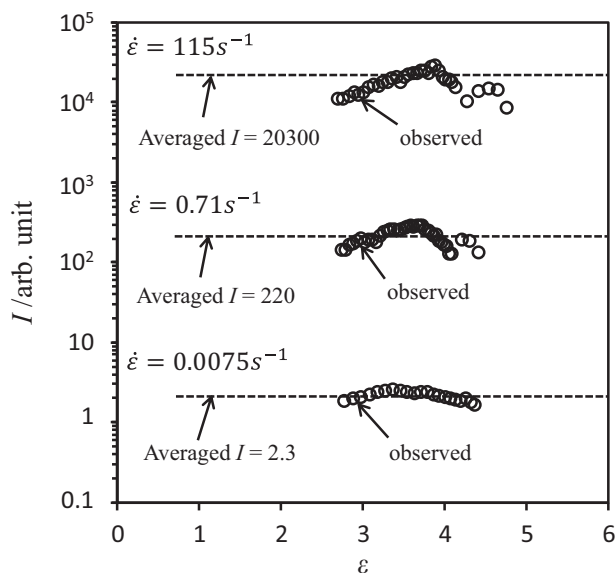
Fig. 7 Plots of I against ε for NR as a function of $\dot{\varepsilon}$

References

1. Lindley PB. Relation between hysteresis and the dynamic crack growth resistance of natural rubber. Int J Fract. 1973;9: 449–62.
2. Hirata, Y, Kondo, H & Ozawa, Y in Chemistry, Manufacture and Application of Natural Rubber (Kohjiya, S & Ikeda, Y ed.) Ch.12, 325-52 (Woodhead Publishing Ltd, Cambridge, 2014).
3. Katz JR. Röntgenspektrographische Untersuchungen am gedehnten Kautschuk und ihre mögliche Bedeutung für das Problem der Dehnungseigenschaften dieser Substanz. Naturwissenschaften. 1925;19:410–6.
4. Lee DJ, Donovan JA. Microstructural changes in the crack tip region of carbon-black-filled natural rubber. Rubber Chem Technol. 1987;60:910–23.
5. Le Cam JB, Toussaint E. The mechanism of fatigue crack growth in rubbers under severe loading: the effect of stress-induced crystallization. Macromolecules. 2010;43:4708–14.
6. Alexander LE, Ohlberg S, Taylor GR. X-ray diffraction studies of crystallization in elastomers. Rubber Chem Technol. 1956;29:438–50.
7. Murakami S, Senoo K, Toki S, Kohjiya S. Structural development of natural rubber during uniaxial stretching by in situ wide angle X-ray diffraction using a synchrotron radiation. Polym (Guildf). 2002;43:2117–20.
8. Chenal JM, Gauthier C, Chazeau L, Guy L, Bomal Y. Parameters governing strain induced crystallization in filled natural rubber. Polym (Guildf). 2007;48:6893–901.
9. Mitchell JC, Meier DJ. Rapid stress-induced crystallization in natural rubber. J Polym Sci Part A-2. 1968;6:1689–703.
10. Candau N, Chazeau L, Chenal JM, Gauthier C, Munch E. A comparison of the abilities of natural rubber (NR) and synthetic polyisoprene cis-1,4 rubber (IR) to crystallize under strain at high strain rates. Phys Chem Chem Phys. 2016;18:3472–81.
11. Tosaka M, Senoo K, Sato K, Noda M, Ohta N. Detection of fast and slow crystallization processes in instantaneously-strained samples of cis-1,4-polyisoprene. Polym (Guildf). 2012;53:864–72.
12. Okada KN, Tagashira K, Sakai K, Masunaga H, Hikosaka M. Temperature dependence of crystallization of nano-oriented crystals of iPP and the formation mechanism. Polym J. 2013;45:70–78.
13. Okada K, Tanaka Y, Masunaga H, Hikosaka M. 3D structure of nano-oriented crystals of poly(ethylene terephthalate) formed by elongational crystallization from the melt. Polym J. 2018;50:167–76.
14. Okada KN, Washiyama J, Watanabe K, Sasaki S, Masunaga H, Hikosaka M. Elongational crystallization of isotactic polypropylene forms nano-oriented crystals with ultra-high performance. Polym J. 2010;42:464–73.
15. Becher VR, Dönig W. Kinetische Behandlung der Keimbildung in übersättigten Dämpfen. Ann Phys. 1935;24:719–52.
16. Frisch HL. Time lag in nucleation. J Chem Phys. 1957;27:90–94.
17. Andres RP, Boudart M. Time lag in multistate kinetics: Nucleation. J Chem Phys. 1965;42:2057–64.
18. Miyamoto Y, Yamao H, Sekimoto K. Crystallization and melting of polyisoprene rubber under uniaxial deformation. Macromolecules. 2003;36:6462–71.
19. Kitamura, Y, Okuno, K, Okada, K & Hikosaka, M. equilibrium melting temperature in oriented melt and strain induced crystallization mechanism of natural rubber. *FSBL 2013 Seika-Houkokusyu*, 51-52 (2013).
20. Kitamura Y, Okada K, Masunaga H, Hikosaka M. Study of Strain Induced Crystallizaion Mechanism in Natural Rubber. Polym Prepr, Jpn. 2015;64:1G13. No.2
21. Kitamura, Y, Okada, K, Masunaga, H & Hikosaka, M. Evidence of nucleation controlled mechanism of strain induced crystallization (SIC) of natural and synthetic isoprene rubber. *manuscript in preparation*.
22. Ogawa H, Masunaga, H, Sasaki, S, Goto, S, Tanaka, T, Seike, T. et al. Experimental station for multiscale surface structural analyses of soft-material films at SPring-8 via a GIWAX/GIXD/XR-integrated system. Polym J. 2013;45:109–16.
23. Masunaga H, Ogawa, H, Tanaka, T, Sasaki, S, Goto, S, Tanaka, T. et al. Multipurpose soft-material SAXS/WAXS/GISAXS beamline at SPring-8. Polym J. 2011;43:471–7.